Raman Spectroscopy of Uracil DNA Glycosylase−DNA Complexes: Insights into DNA Damage Recognition and Catalysis†

Jian Dong,‡ Alexander C. Drohat,§ James T. Stivers,§ Kryzsztof W. Pankiewicz,|| and Paul R. Carey*,‡

Department of Biochemistry, Case Western Reserve University, 10900 Euclid Avenue, Cleveland, Ohio 44106-4935, Center for Advanced Research in Biotechnology of the University of Maryland Biotechnology Institute and the National Institute of Standards and Technology, 9600 Gudelsky Drive, Rockville, Maryland 20850, and Pharmasset, Inc., 1860 Montreal Road, Tucker, Georgia 30084

Received June 23, 2000; Revised Manuscript Received August 8, 2000

ABSTRACT: Using off-resonance Raman spectroscopy, we have examined each complex along the catalytic pathway of the DNA repair enzyme uracil DNA glycosylase (UDG). The binding of undamaged DNA to UDG results in decreased intensity of the DNA Raman bands, which can be attributed to an increased level of base stacking, with little perturbation in the vibrational modes of the DNA backbone. A specific complex between UDG and duplex DNA containing 2′-β-fluorodeoxyuridine shows similar increases in the level of DNA base stacking, but also a substrate-directed conformational change in UDG that is not observed with undamaged DNA, consistent with an induced-fit mechanism for damage site recognition. The similar increases in the level of DNA base stacking for the nonspecific and specific complexes suggest a common enzyme-induced distortion in the DNA, potentially DNA bending. The difference spectrum of the extrahelical uracil base in the substrate−analogue complexes reveals only a small electron density reorganization in the uracil ring for the ground state complex, but large 34 cm^{-1} downshifts in the carbonyl normal modes. Thus, UDG activates the uracil ring in the ground state mainly through H bonds to its C═O groups, without destroying its quasi-aromaticity. This result is at variance with the conclusion from a recent crystal structure, in which the UDG active site significantly distorts the flipped-out pseudouridine analogue such that a change in hybridization at C1 occurs [Parikh, S. S., et al. (2000) *Proc. Natl. Acad. Sci. USA 97*, 5083]. The Raman vibrational signature of the bound uracil product differs significantly from that of free uracil at neutral pH, and indicates that the uracil is anionic. This is consistent with recent NMR results, which established that the enzyme stabilizes the uracil anion leaving group by 3.4 pK_a units compared to aqueous solution, contributing significantly to catalysis. These observations are generally not apparent from the high-resolution crystal structures of UDG and its complexes with DNA; thus, Raman spectroscopy can provide unique and valuable insights into the nature of enzyme−DNA interactions.

In recent years, there have been considerable advances in our understanding of the structural biology of enzymatic repair of damaged DNA. The availability of high-resolution crystal structures of many enzymes, and their specific complexes with various types of damaged DNA, have led to detailed models of the interactions that lead to specific recognition and catalysis (*1*). Although such structures provide invaluable static snapshots of stable species along the reaction pathway, crystallography is often not well suited to the study of weak nonspecific DNA−enzyme complexes, unstable enzyme-bound intermediates, or conformational states that are in dynamic equilibrium in solution. Thus, alternative high-resolution approaches are desirable for gaining a fuller understanding of these transient complexes during enzymatic repair of damaged DNA. To probe these questions, we have been utilizing NMR, fluorescence, and, in this account, Raman spectroscopy.

Perhaps the most structurally and mechanistically well-characterized DNA repair enzyme is uracil DNA glycosylase (UDG),[1] the first enzyme involved in the uracil base excision repair pathway (*2*). UDG cleaves the glycosidic bond of deoxyuridine in both double-stranded and single-stranded DNA using a simple hydrolytic mechanism, involving water attack at the C1′ position of deoxyuridine (*3*). Many aspects of damaged site recognition and catalysis have been addressed in detail for the *Escherichia coli* enzyme (*3*−*7*)

† This work was supported by NIH Grants RO1 GMS56834 (J.T.S.) and GM-54072 (P.R.C.) and the National Institute for Standards and Technology. A.C.D. is a National Research Council Postdoctoral Associate.

* To whom correspondence should be addressed. Phone: (216) 368-0031. Fax: (216) 368-3419. E-mail: carey@biochemistry.cwru.edu.

‡ Case Western Reserve University.

§ Center for Advanced Research in Biotechnology of the University of Maryland Biotechnology Institute and the National Institute of Standards and Technology.

|| Pharmasset, Inc.

[1] Abbreviations: dsAB, double-stranded 11mer DNA containing a tetrahydrofuran abasic site; dsU^{β}, double-stranded 11mer DNA containing 2′-β-fluorodeoxyuridine; dsT, double-stranded 11mer DNA containing 2′-deoxythymidine; d$^{\psi}$U, 2′-deoxypseudouridine; *e*UDG, *E. coli* uracil DNA glycosylase; ssAB, single-stranded 4mer DNA with the sequence A*F*AA, where *F* denotes a tetrahydrofuran abasic site; ssAU$^{\beta}$AA, single-stranded 4mer DNA containing 2′-β-fluoro-2′-deoxyuridine.

10.1021/bi001437m CCC: $19.00
Published on Web 10/07/2000

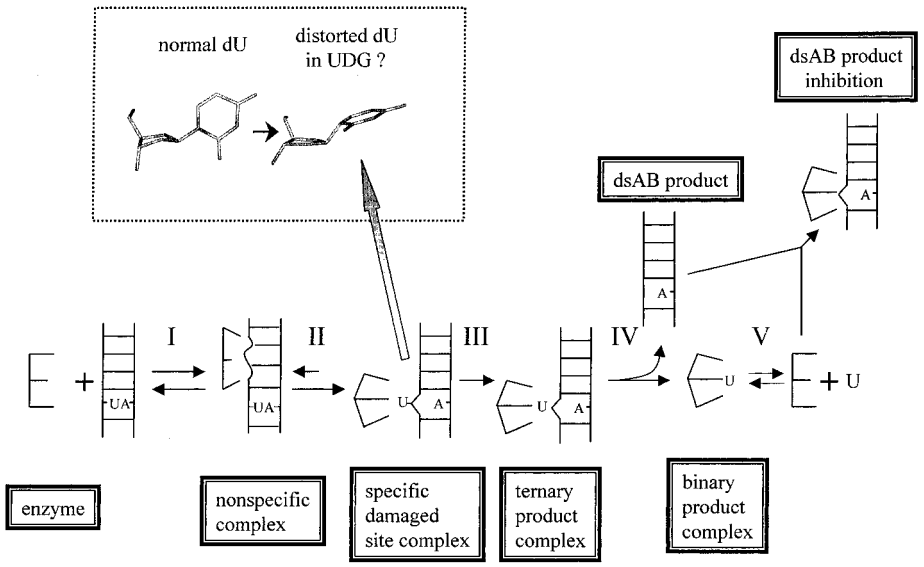

FIGURE 1: Complexes along the reaction pathway of uracil DNA glycosylase. Many of the rate constants and equilibrium constants have been determined for *e*UDG (*3*, *7*). A minimum of five steps are required: (step I) nonspecific binding to DNA, which is envisioned to involve DNA strain or local bending (*7*); (step II) specific binding at the damage site, which entails flipping of the uracil base from the DNA helix and induced-fit changes in UDG (*7*); (step III) cleavage of the glycosidic bond to produce uracil and abasic DNA; (step IV) release of the abasic DNA product; and (step V) uracil release. As indicated, the abasic DNA product can bind to UDG in a competitive manner with substrate DNA (*24*). The unusual tetrahedral geometry that is suggested for the glycosidic bond of flipped enzyme-bound deoxyuridine is illustrated (*8*).

(*e*UDG) (Figure 1). Rapid kinetic measurements of uracil recognition by *e*UDG have shown that the first step is diffusion-controlled and weak nonspecific binding of the enzyme with undamaged DNA, followed by a rapid step ($\sim$1000 s^{-1}) in which the damaged uracil base is extruded from the DNA helix (*7*). Currently, there is no crystal structure of a complex between UDG and undamaged DNA. However, Tainer and colleagues have recently determined the structure of *h*UDG bound to a duplex DNA containing the stable C-glycoside substrate analogue 2′-deoxypseudouridine ($d^{\psi}U$) (*8*). One remarkable observation in this structure was that the normally trigonal planar geometry of the C1 atom of $d^{\psi}U$ (corresponding to N1 in dU) was bent toward a tetrahedral geometry. In addition, the uracil ring plane was rotated on its glycosidic bond axis by 90° from its normal torsion angle to an orientation almost parallel to the deoxyribose ring plane (Figure 1 inset). It was argued that such a strained conformation, if effected in the natural substrate, would lead to enhanced electron orbital overlap between the glycosidic bond and the π-systems of the uracil ring, and promote a dissociative transition state for glycosidic bond cleavage. This presumed stereoelectronic effect was characterized as the key aspect of catalysis, thereby explaining a majority of the 10^{12}-fold catalytic power of UDG (*8*).

However, comprehensive heteronuclear NMR and mutagenesis experiments on *e*UDG have indicated a significant role for chemical catalysis in the reaction. A role for electrophilic catalysis by the completely conserved His187 has been established (*3*−*5*). This neutral electrophile has been shown to interact weakly with the substrate in the ground state complex, but forms a short strong hydrogen bond with uracil O2 in the ternary product complex (corresponding to His268 in Scheme 1 for the human enzyme), and presumably the transition state as well. This hydrogen bond, together with other active site interactions, lowers the N1 pK_a of the uracil leaving group by 3.4 units as compared to solution

Scheme 1: Binding of DNA in Human UDG, Showing the Flipped-Out Nucleotide and the Cleaved N−C1′ Glycosidic Bond (*9*)

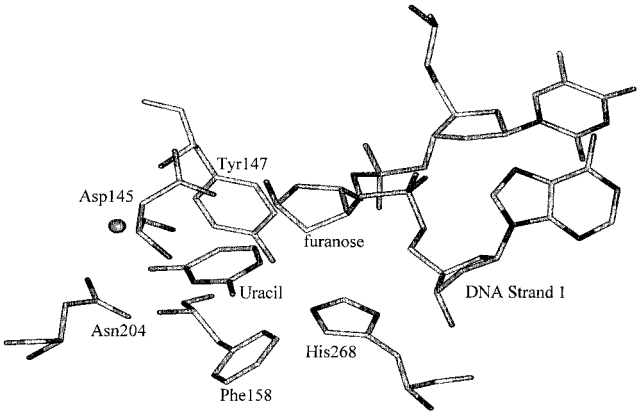

(*5*). Accordingly, the uracil base is bound as the anion at physiological pH, an important aspect of catalysis that was not revealed by the high-resolution crystal structures of the human enzyme (*h*UDG) bound to the products abasic DNA and uracil (*9*). A comparable energetic role for the active site aspartic acid (Asp64) in deprotonating or positioning the attacking water nucleophile has also been indicated from structural, NMR, and kinetic studies (*3*−*5*). In addition, as shown in Figure 1, the final steps in catalytic turnover are ordered release of the abasic DNA product followed by uracil. The binary product complexes are also structurally well characterized, with high-resolution structures of *e*UDG bound to uracil (*4*, *6*) and *h*UDG bound to abasic DNA available (*9*).

In this study, we use Raman spectroscopy to probe the nature of each complex along the reaction pathway of UDG (Figure 1). The high sensitivity of the Raman signal for changes in DNA base stacking interactions, and the electronic features of the uracil base when bound in the enzyme active

site, provides valuable mechanistic information that is not readily obtained by other approaches.

EXPERIMENTAL PROCEDURES[2]

Materials. Wild-type UDG from *E. coli* strain B was produced using a T7 polymerase-based expression system and purified to >99% homogeneity as described previously (*6*, *10*). The concentration of UDG was determined using the relationship $\epsilon^{280} = 38\,511\ mM^{-1}\ cm^{-1}$ (*10*). The 0.5 mM UDG stocks were in 10 mM NaH_2PO_4 and 0.2 M NaCl, and were adjusted to pH 7.5.

The three duplex 11mer DNAs used in these experiments contained the sequence 5′-GCGCA***X***AGTCG-3′, where ***X*** denotes either a tetrahydrofuran abasic site, 2′-β-fluoro-2′-deoxyuridine, or 2′-deoxythymidine, and the complementary sequence 5′-CGACTATGCGC-3′. The oligonucleotides were synthesized, purified, and characterized essentially as described previously (*3*, *7*), including characterization by MALDI-TOF mass spectrometry. The 4mers AU$^{\beta}$AA and A*F*AA were obtained using the same procedures. The concentrations were determined by UV absorption measurements at 260 nm, using the pairwise extinction coefficients for the constituent nucleotides (*11*). The duplex DNA was hybridized as previously described (*7*), except that the buffer was 10 mM NaH_2PO_4 (pH 7.5) and 0.1 M NaCl.

The dsAB and A*F*AA (ssAB) DNA used in these studies contained a tetrahydrofuran abasic site analogue (phosphoramidite from Glen Research, Sterling, VA). Although this analogue differs slightly from the abasic site of the natural product in that a 1′-hydrogen replaces the 1′-hydroxyl group, the same highly deshielded resonance arising from the hydrogen bond between His187 and uracil O2 is observed for the ternary product complex formed with both types of abasic sites (*12*) which indicates that this difference does not effect the active site structure in the product complex.

Raman Spectroscopy. For the enzyme complexes, Raman spectra were acquired using 1 W, 647.1 nm laser excitation from an Innova 400 krypton laser (Coherent, Inc.) and a modified Holospec f/1.4 axial transmission spectrometer (*13*). Typically, sample volumes were 50 μL, and the spectrum was recorded at 20 °C with the data collection time of 5 min per spectrum. The spectrum of the enzyme with a stoichiometric amount of uracil and/or DNA duplex was recorded immediately after recording the spectrum of the enzyme. The subtraction of [enzyme + ligand] minus [enzyme] gave the spectrum of the bound ligand. The computer subtraction was undertaken using Grams/32 software (Galactic Industries, Inc.). Several factors contribute to the stability of our Raman instrumentation and assist us in undertaking accurate differential experiments (*13*, *14*). Neither the sample arrangement nor any optical component (grating or lenses) inside the spectrograph moves during data acquisition, ensuring that the images of the two parent spectral signals do not undergo a displacement with respect to each other.

[2] Certain commercial equipment, instruments, and materials are identified in this paper to specify the experimental procedure. Such identification does not imply recommendation or endorsement by the National Institute of Standards and Technology, nor does it imply that the material or equipment identified is necessarily the best available for the purpose.

Quantum mechanical computations have been performed to analyze the vibrational assignments of the product uracil and the β-isomer of 2′-fluoro-2′-deoxyuridine nucleoside in various ionization and ribose ring conformational states, using the Gaussian98 code (*15*). The full geometry optimization of the molecules was carried out without freezing any degree of conformational freedom for the subsequent estimation of harmonic force constants at the same density functional theory (DFT) level (B3LYP method). A Gaussian basis set of 6-31+G(d,p) under the Onsager reaction field model was used for various uracil species in the dielectric constant media of water ($\epsilon = 78.39$), while a Gaussian basis set of 6-31G* was used for the 2′-deoxy-2′-fluoro-*arabino*-furanosyluridine. The absence of imaginary wavenumbers confirmed that the optimized geometries correspond well to the ground state energy minima and not to a saddle point of the potential energy surface. The raw (unscaled) wavenumbers are reported, along with their assignments and Raman intensities. No scaling factors have been used to improve the agreement between the experimental and theoretical values, because the DFT method is now generally considered to be a suitable theoretical basis for reproducing band wavenumbers and intensities.

RESULTS AND DISCUSSION

UDG Interactions with Undamaged DNA

Raman Spectra of Free UDG and Free DNA. The Raman spectrum of free UDG, excited at 647.1 nm, is shown in Figure 2A. The assignments of the major bands, shown under the spectrum, are in accord with the literature (*16*), and more detailed assignments are listed in Table 1 of the Supporting Information. The appearance of the amide I maximum at 1656 cm^{-1} and the high relative intensities near 1342 and 945 cm^{-1} are evidence for a substantial fraction of α-helical secondary structure (*17*), which is consonant with the 32% α-helical content observed in the X-ray crystal structure of *e*UDG (*6*). The amide I region and several of the aromatic amino acid side chain modes seen in Figure 2A will become important in the discussion of Raman difference spectroscopic data below.

The Raman spectrum of undamaged dsT DNA is shown in Figure 2B along with the assignments for the major peaks (see also Table 2 of the Supporting Information). The Raman markers at 833 and 1093 cm^{-1} (due to the phosphodiester O−P−O stretching) are diagnostic of canonical B-DNA (*18*), and the bands at 683 (dG), 732 (dA), and 788 cm^{-1} (dC) identify C2′-*endo/anti* deoxynucleotide (*19*).

The Raman features of free dsT are very similar to those of the other double-stranded DNAs used in these studies: (i) dsU$^{\beta}$ (Figure 3D), in which the central dT nucleotide is replaced with 2′-β-fluorodeoxyuridine, and (ii) dsAB, in which the dT is replaced with an abasic site (data not shown). These similar features indicate that each of these 11mer duplex DNAs adopts an indistinguishable B-DNA structure. As will be discussed below, the Raman spectral features of B-DNA are highly sensitive to the changes in base stacking and base pairing interactions that can occur upon binding of a protein or enzyme.

UDG Increases the Level of Base Stacking Interactions upon Binding DNA. Figure 3A shows the Raman spectrum

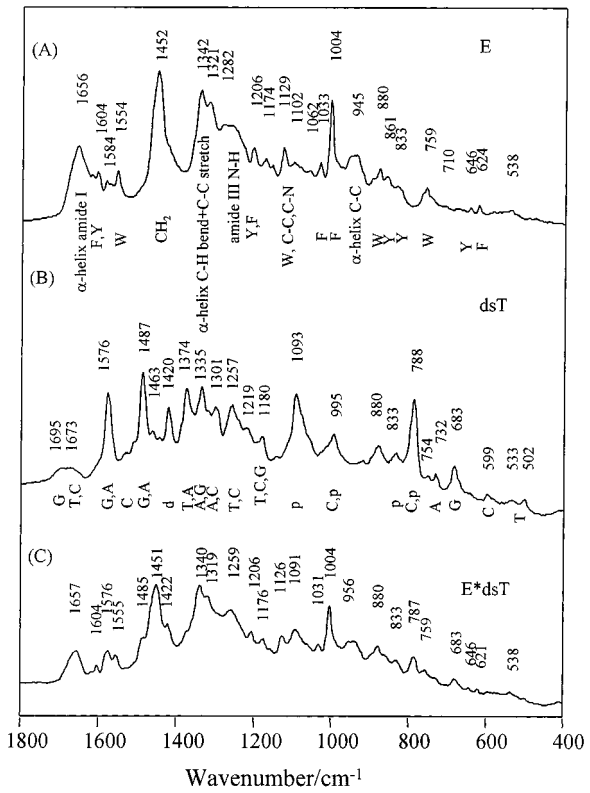

FIGURE 2: Raman spectrum of (A) 490 μM UDG (E), (B) 0.60 mM dsT, and (C) the UDG−dsT complex (0.93:1.0 [dsT]:[UDG], [UDG] = 0.49 mM). Under the experimental conditions that were used, 1 W of laser power and 5 min data collection time, the intense peak near 1452 cm^{-1} in the spectrum of UDG corresponds to approximately 2.3×10^6 photon events, and the intense features in the spectrum of dsT represent approximately 10^6 photon events. The samples contained 10 mM sodium phosphate buffer (pH 7.5) and 150 mM NaCl. The spectrum of the buffer alone was subtracted from the spectrum of UDG, dsT, and the complex.

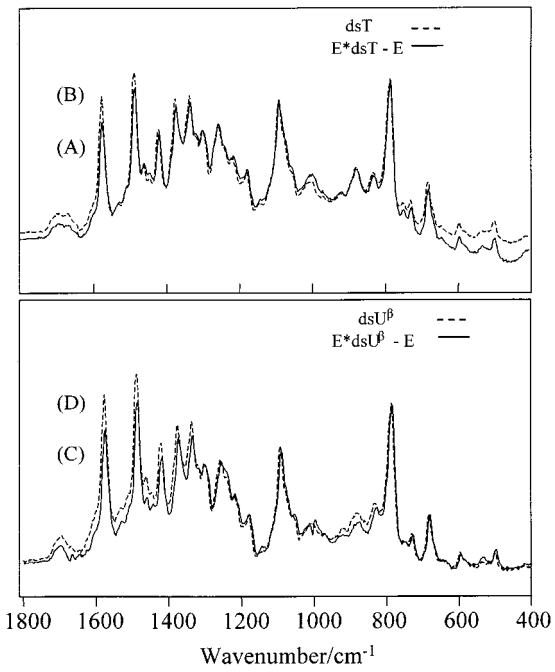

FIGURE 3: (A) Raman spectrum of dsT bound to UDG obtained by subtracting the enzyme spectrum from the spectrum of the E−dsT complex (solid line) (0.93:1.00 [dsT]:[UDG], [UDG] = 0.49 mM). (B) Raman spectrum of free dsT (0.60 mM) in aqueous solution (dashed line). The intensities in spectrum B are scaled to the same concentration level as in spectrum A. (C) Raman spectrum of dsU^β substrate bound to UDG obtained by subtracting the enzyme spectrum from that of the E−dsU^β complex (solid line). The [dsU^β]:[UDG] ratio was 0.93:1.00, and [UDG] = 0.49 mM. The data were acquired within 10 min of formation of the complex. (D) Raman spectrum of free dsU^β (0.60 mM) in aqueous solution (dashed line). The intensities in spectrum D are scaled to the same concentration level as in spectrum C. All samples were buffered in 10 mM sodium phosphate and 150 mM NaCl (pH 7.5).

of dsT bound to UDG, which was acquired by subtracting the spectrum of the free enyme from the spectrum of the complex (i.e., E−dsT − E). For comparison, the spectrum of free dsT is shown overlaid with the spectrum of the complex (Figure 3B). A decrease in Raman intensity occurs for several bands in the nonspecific E−dsT complex; most significantly, the intensities of the bands at 1577 and 1488 cm^{-1} decrease by ca. 20% (this measurement is made when both spectra are baseline corrected). This can be better seen in the difference spectrum shown in Figure 4A, which was obtained by subtracting the spectra of free dsT and free UDG from the spectrum of the E−dsT complex. The dominating "negative" ring modes of the bases indicate that an increase in base stacking occurs upon nonspecific binding of undamaged DNA to UDG.

Nature of UDG-Damaged DNA Complexes before Glycosidic Bond Cleavage

Conformational Changes in dsU^β DNA. The substitution of fluorine for the 2′-β-hydrogen in deoxyuridine renders it resistant to base excision by UDG ($t_{1/2} \sim 20$ h in ds DNA) (*7*), which allowed us to examine the specific complex of UDG bound to DNA containing a damaged uracil site. The 11mer ds DNA used in these studies, dsU^β, was identical to the undamaged dsT, except that dU^β replaced the central dT nucleotide. Figure 3C shows the difference Raman spectrum of dsU^β bound to UDG, which was acquired by subtracting the spectrum of UDG from the spectrum of the complex (i.e., E−dsU^β − E). This spectrum was obtained within 10 min of forming the complex, such that hydrolysis of the *N*-glycosidic bond of dsU^β was negligible (*7*). For comparison, the spectrum of free dsU^β is shown overlaid with the spectrum of the complex (Figure 3D).

As was seen for the undamaged dsT DNA, a decrease in intensity occurs for several bands in the Raman spectrum of the dsU^β DNA upon binding UDG, most prominently at 1577 and 1488 cm^{-1}. This can be more clearly seen in the difference spectrum in Figure 4B, obtained by subtracting the spectrum of free dsU^β and free UDG from the spectrum of the dsU^β−UDG complex. This spectrum is dominated by negative ring modes for the bases, with the intensities of the bands near 1577 and 1488 cm^{-1} decreasing by about 20% (detailed assignments are given in Table 2 of the Supporting Information). The Raman hypochromism observed in this spectrum indicates an increase in the level of base stacking interactions for dsU^β upon binding UDG. Thus, any decrease in the level of base stacking caused by uracil flipping is overwhelmed by the increase in the level of base stacking throughout the rest of the DNA. In addition, there is no evidence for a large conformational change in the DNA backbone for the damage specific complex, although the weak peak observed for the 1095 cm^{-1} marker may reflect a local change near the flipped-out dU^β nucleotide. This is

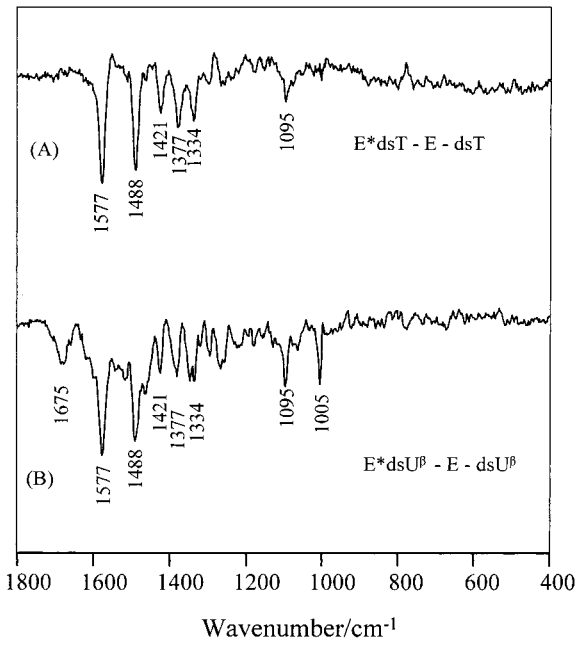

FIGURE 4: Comparison of Raman difference spectrum of (A) dsT and (B) dsU$^{\beta}$, showing intensity changes of the bases before and after binding to UDG. In each spectrum, the Raman spectrum of free dsU$^{\beta}$ or dsT in aqueous solution (Figure 3D or 3B) was taken as a reference, and subtracted from that of the bound spectrum (Figure 3C or 3A). The data were scaled as described in the caption of Figure 3.

in strong contrast to the major changes in the DNA backbone observed recently by Benevides et al. for a target B-DNA sequence bound to the high-mobility group box protein (*20*).

Is DNA Bending a Common Feature of the Nonspecific and Damage Specific Complexes? The similar increases in the level of DNA stacking observed for dsT and dsU$^{\beta}$ upon binding UDG, and the lack of significant DNA backbone conformational changes, reflect common features in the nonspecific and damage specific complexes. We have previously proposed a mechanism for base flipping by UDG that included an enzyme-induced destabilization of the DNA duplex upon forming the nonspecific encounter complex, followed by a fast uracil flipping step (*7*). Such a mechanism could account for the observation that the uracil flipping rate was independent of base pair stability (i.e., U$^{\beta}$·G and U$^{\beta}$·A base pairs and single-stranded U$^{\beta}$ DNA showed the same rate of base flipping into the UDG active site). Although it is difficult to interpret the energetic implications of the increased level of base stacking observed for these complexes, this spectral feature may represent enzyme-induced strain or bending in the DNA helix that serves to facilitate the uracil-flipping step. Indeed, it has been reported that B-DNA cannot be docked into the active site of the UDG without bending (*9*).

Binding of dsU$^{\beta}$ Induces a Conformational Change in UDG. In contrast with the similar DNA conformational changes that are observed upon UDG binding of undamaged and substrate analogue DNA, only dsU$^{\beta}$ appears to induce a conformational change in UDG. The appearance of the amide I-like negative feature near 1675 cm^{-1} in Figure 4B indicates a slight perturbation in a β-sheet motif of the enzyme upon forming the complex. Given the complex nature of the amide I profile, it is difficult to quantitate the change in secondary structure giving rise to the 1675 cm^{-1} Raman difference feature. However, the observation of a perturbation to the β-sheet region is remarkably consistent with the crystallographic observation that the β-sheet interaction between the β1 and β3 strands is extended by two residues upon specific DNA binding (*21*). The sharp negative peak at 1005 cm^{-1}, which can be assigned with confidence to a phenylalanine side chain mode, exhibits decreased intensity upon complex formation. We ascribe this to the stacking interaction between the substrate uracil base and the Phe77 side chain, as seen in X-ray crystal structures (Scheme 2) (*6*, *9*). The decreased intensity of the Phe77 side chain upon stacking with the quasi-aromatic uracil base is analogous to the Raman hypochromism discussed above for the bases in the DNAs. These changes are not seen for the E−dsT complex; thus, we are detecting a substrate-induced perturbation of an individual Phe residue in the active site, one of the 11 Phe residues in the enzyme.

Observing the Flipped-Out Uracil Base Prior to Cleavage of the Glycosidic Bond

Raman Signature of the Extrahelical Uracil Base. To examine the Raman signature of the uracil base alone, within the context of free dsU$^{\beta}$, and flipped into the active site of UDG, we undertook a series of difference Raman experiments. In the first experiment (Figure 5A), the Raman signature of the uracil base within free dsU$^{\beta}$ was acquired by subtracting the spectrum of dsAB from the spectrum of

Scheme 2: Active Site Interactions in *e*UDG before and after Binding of the Uracil Ligand (*6*)

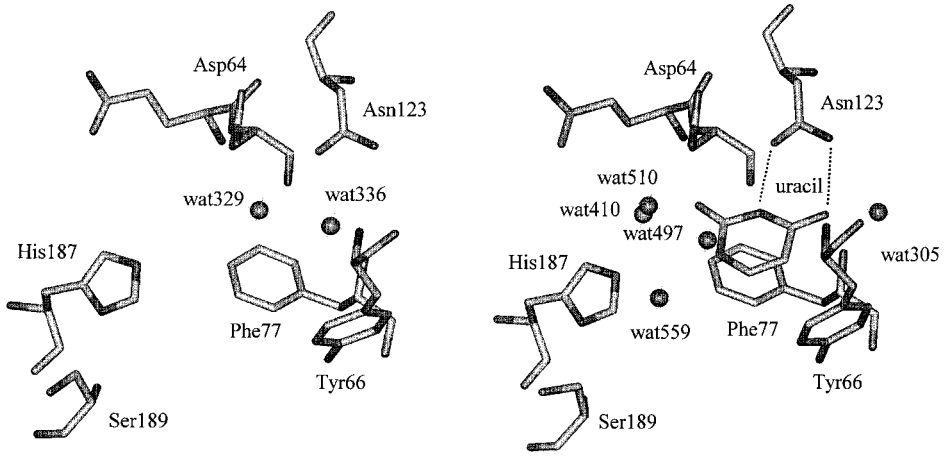

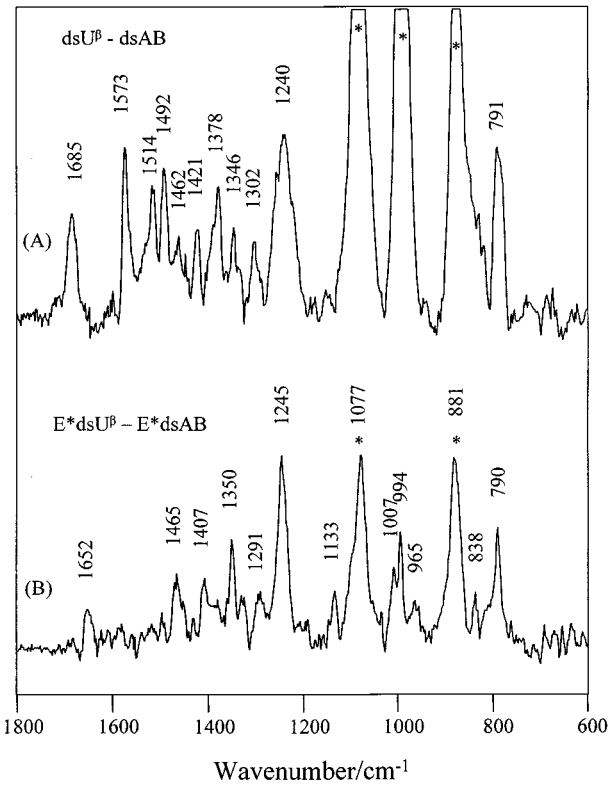

FIGURE 5: (A) Raman spectrum of the uracil base within dsU$^{\beta}$ (0.60 mM), generated by subtracting the Raman spectrum of free dsAB from that of free dsU$^{\beta}$. (B) The Raman signature of the uracil within dsU$^{\beta}$ bound to the UDG active site, acquired by subtracting the Raman spectrum of dsAB bound to UDG from that of dsU$^{\beta}$ bound to UDG. The ratio of the dsU$^{\beta}$ or dsAB concentration to the UDG concentration was 9:10, and [UDG] = 490 μM. All samples were buffered in 10 mM sodium phosphate and 150 mM NaCl (pH 7.5). The peaks with asterisks are due to phosphate buffer that have not been subtracted to zero.

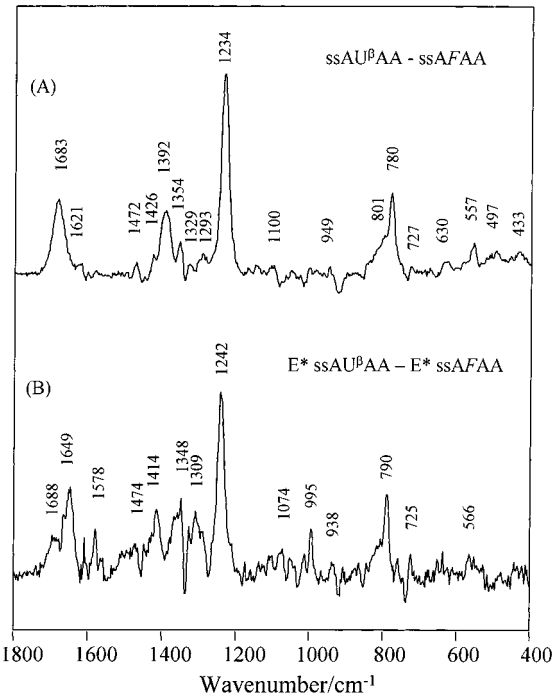

FIGURE 6: (A) Raman signature of uracil base within ssAU$^{\beta}$AA (1.0 mM), generated by subtracting the Raman spectrum of the single-stranded abasic DNA tetramer (ssA*F*AA) from that of free ssAU$^{\beta}$AA. (B) The Raman spectrum of the uracil base in ssAU$^{\beta}$AA bound to the UDG active site, acquired by subtracting the Raman spectrum of ssA*F*AA bound to UDG from that of ssAU$^{\beta}$AA bound to UDG. The ratio of the ssAU$^{\beta}$AA or ssA*F*AA concentration to the UDG concentration was 0.8:1.0. The UDG concentration was 0.5 mM, and all the samples were buffered in 10 mM sodium phosphate and 200 mM NaCl (pH 7.5).

dsU$^{\beta}$ DNA (dsAB is identical to dsU$^{\beta}$ except for an abasic site replacing U$^{\beta}$). The uracil base in free dsU$^{\beta}$ is characterized by the Raman difference bands at 1685, 1378, 1240, and 791 cm^{-1}. The bands at 1573, 1514, 1492, 1346, and 1302 cm^{-1} are assigned to adenine modes, and probably arise from the different environments of the adenine base that is paired with uracil in dsU$^{\beta}$, but is orphaned in the abasic DNA. It is often observed that unpaired bases have a Raman profile that is distinct from that of the paired base in B-DNA (*22*).

In the second experiment (Figure 5B), the Raman signature of the uracil base within dsU$^{\beta}$ while flipped into the enzyme active site was obtained by subtracting the spectrum of the E−dsAB complex from the spectrum of the E−dsU$^{\beta}$ complex. Interestingly, most of the bands due to the adenine base in Figure 5A disappear in Figure 5B when dsU$^{\beta}$ is bound to UDG, indicating the formation of an orphan adenine base in the enzyme−substrate complex, in accord with the base flipping mechanism. Two features of the uracil base of bound dsU$^{\beta}$ are seen clearly at 1245 and 790 cm^{-1} in Figure 5B. The 1245 cm^{-1} band is a complex feature arising from coupled uracil ring and N_1-C_1' stretching, as well as a C_5-H in-plane bending mode, while the 790 cm^{-1} feature is due to a ring breathing mode (J. Dong and P. R. Carey, unpublished results). There are only small shifts in these features of the uracil base when dsU$^{\beta}$ is bound to UDG, which indicates only a minor electronic reorganization of the uracil ring upon forming the ground state complex. This conclusion is supported fully by the additional experiments with single-stranded AU$^{\beta}$AA below.

Ground State Destabilization of the N-Glycosidic Bond via H Bonding. To obtain higher-quality data that focus primarily on the interactions of the uracil base in the active site of UDG, we also obtained difference Raman spectra for the single-stranded 4mer DNA, AU$^{\beta}$AA, both free and bound to UDG. Figure 6A shows the Raman signature of the uracil base within ssAU$^{\beta}$AA, which was obtained by subtracting the spectrum of the single-stranded A*F*AA (ssAB) from the spectrum of single-stranded AU$^{\beta}$AA (A*F*AA is identical to AU$^{\beta}$AA but with a tetrahydrofuran abasic site replacing U$^{\beta}$). The Raman signature of the uracil base within AU$^{\beta}$AA when flipped into the active site was obtained by subtracting the spectrum of the E−ssAB complex from the spectrum of the E−ssAU$^{\beta}$AA complex (Figure 6B). As shown in Figure 6B, the binding of AU$^{\beta}$AA to UDG brings about fairly large changes in the C=O stretching region between 1600 and 1700 cm^{-1}, but only modest changes in the position of the two intense ring modes near 1240 and 790 cm^{-1} (upshifts of 8 and 10 cm^{-1}, respectively). This indicates that the structure and electron distribution of the uracil ring undergo only a minor perturbation on going from solution to the active site of UDG. This result is in marked contrast to the crystallographic findings of Parikh et al. (*8*), who suggested that the substrate analogue deoxypseudouridine undergoes a major distortion in the active site of UDG such that the glycosidic C1 atom of the pseudouridine ring (corresponding to N1 in deoxyuridine) pyramidalizes (Figure 1). If such a

profound effect occurred in the complexes studied here, there should be a radical rearrangement of the uracil ring modes, because the normal mode makeup of the 1240 and 790 cm^{-1} bands should be highly sensitive to such changes in geometry (see above). Thus, the data presented here provide no evidence that UDG uses extreme conformational strain to lower the activation barrier for glycosidic bond cleavage.

A likely source of catalytic power is suggested by the large downshifts in the uracil carbonyl frequencies upon binding to UDG (compare spectra A and B of Figure 6). The uracil carbonyl features in free ssAU$^{\beta}$AA contribute to a broad band at 1683 cm^{-1} that results from two overlapped C═O normal modes, each comprised of a coupled C2═O and C4═O vibration. These modes are replaced by peaks at 1649 and 1688 cm^{-1} in the E−ssAU$^{\beta}$AA complex (Figure 6B), indicating relatively strong hydrogen bonds to the carbonyls in the active site ($\Delta\nu = 34$ cm^{-1}). Similar effects are also seen for the double-stranded complex in Figure 5. These ground state hydrogen bonds are attributed to the backbone amide of Gln63, which hydrogen bonds to uracil O2, and/or the side chain amide of Asn123, which interacts with uracil O4 (*6*). A likely role for these hydrogen bonds, in addition to substrate recognition, is to destabilize the *N*-glycosidic bond in the ground state. In contrast, the short hydrogen bond from the side chain imidazole of His187 to uracil O2 has been shown to exert its binding energy entirely in the transition state (*4*). Thus, UDG uses hydrogen bonding in two distinct ways that serve to lower the activation barrier: destabilization of the glycosidic bond in the ground state and stabilization of the negative charge on uracil O2 in the transition state by recruitment of His187.

UDG Interactions with the Uracil and dsAB Products

Reference Spectra of Neutral Uracil and Its Monoanions. Figure 7 shows the Raman spectra of free uracil at pH 7.5, where it is neutral, and at pH 10.5, where it carries a single negative charge corresponding to the loss of a proton from either N1 or N3 of the uracil ring (pK_a^{app} values of ∼9.4). Thus, spectra A and B of Figure 7 provide Raman markers for neutral uracil and its monoanion, respectively, with the spectrum at pH 10.5 containing contributions from both the N1 and N3 monoanions. To interpret these spectra, density functional theory calculations were undertaken on the neutral and two anionic forms, and the results are shown in Table 1. The salient result is that the intense feature at 1234 cm^{-1} for neutral uracil is absent in both anionic forms. The calculations also predict that the intense uracil breathing modes for the two monoanions differ by about 35 cm^{-1} (797 cm^{-1} for N1 and 762 cm^{-1} for N3; see Table 1). These predictions are borne out by experiment, as the intense 1234 cm^{-1} band seen for neutral uracil in Figure 7A is absent in Figure 7B for the monoanions. In Figure 7B, the 800 cm^{-1} peak and the unresolved shoulder near 785 cm^{-1} in Figure 7B are likely due to the N1 and N3 anions, respectively.

UDG Lowers the N1 pK_a of Uracil. The Raman signatures of uracil when bound to the active site of UDG at pH 7.5 and 10.2 are shown in spectra C and D of Figure 7, respectively. These spectra were obtained by subtracting the spectrum of free UDG from the spectrum of the UDG−uracil complex (i.e., E−U − E) and contain contributions from uracil modes (above the baseline) and from protein modes

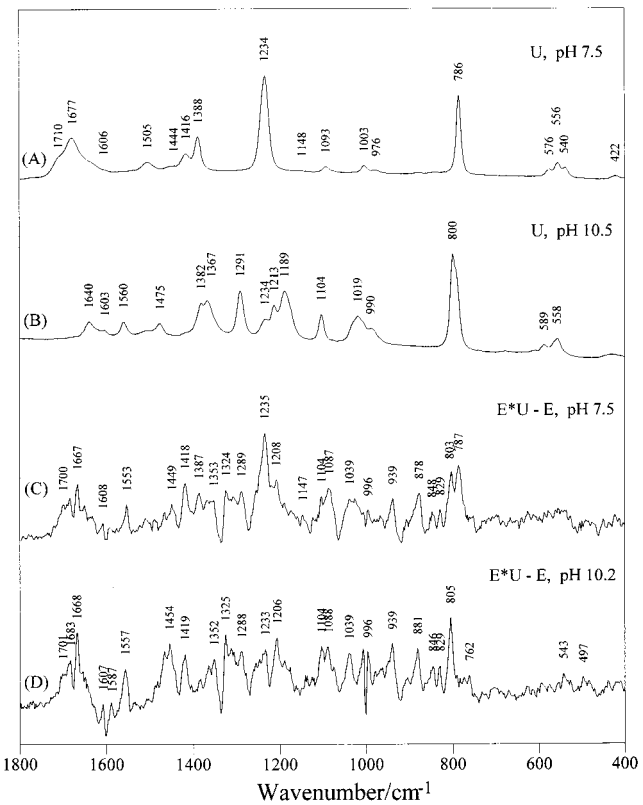

FIGURE 7: Raman spectra of neutral and anionic free uracil and enzyme-bound uracil. (A) Free uracil (12.4 mM) at pH 7.5. (B) Free uracil (10.4 mM) at pH 10.5. (C) Uracil bound to UDG (0.43 mM) at pH 7.5. The spectrum of UDG at pH 7.5 was subtracted from that of the uracil−UDG binary complex. The [UDG]:[uracil] ratio was 1.0:0.9. (D) Uracil bound to UDG (0.46 mM) at pH 10.2. The spectrum of UDG at pH 10.2 was subtracted from that of the uracil−UDG binary complex. The [UDG]:[uracil] ratio was 1.0:0.9. The intensity of these difference peaks is generally about 50 000 photon events, corresponding to about 5% of the original protein signals.

that are perturbed by uracil binding (above or below the baseline). At first sight, some of the features in Figure 7C could be dismissed as "noise"; however, the spectrum is highly reproducible since multiple samples superimpose with great fidelity. The peak at 803 cm^{-1} in the E−U complex at pH 7.5 (Figure 7C) is close to that of the ring breathing mode of the uracil N1 monoanion (Figure 7B), while the intense uracil ring modes near 1235, 1387, and 787 cm^{-1} are characteristic of neutral uracil (Figure 7A). Thus, the bound uracil base appears to be a nearly equal mixture of the neutral and anionic forms at pH 7.5. This observation is entirely consistent with recent NMR results, which indicated that the N1 proton of enzyme-bound uracil has a pK_a of 7.6 (*12*). This N1 pK_a is lowered by 2.2 units compared to that of free uracil, but is 1.2 units higher than that of uracil in the ternary complex with duplex abasic DNA (*5*). Accordingly, there is no evidence for the neutral form of uracil in the Raman spectra of the E−U complex at pH 10.5, as judged by the absence of the neutral marker bands at 1234 and 1388 cm^{-1} in Figure 7D.

It has been demonstrated previously using solution NMR methods that uracil O2 forms a short strong hydrogen bond with the imidazole of the active site His187 in the ternary complex with dsAB DNA, which dramatically lowers the N1 pK_a of uracil by stabilizing the negative charge on O2

Table 1: Density Functional Theory-Predicted Harmonic Frequencies (in cm^{-1}), Raman Intensities (in brackets), and Normal Modes of Neutral Uracil and Its Anions in the Dielectric Constant Media of Water ($\epsilon = 78.39$) in the Wavenumber Region of 2000−400 cm^{-1} [a]

neutral uracil			uracil monoanion				
			uracil N1 anion		uracil N3 anion		
calcd frequency (intensity)	normal mode	observed (cm^{-1})	calcd frequency (intensity)	normal mode	calcd frequency (intensity)	normal mode	observed (cm^{-1})
405.5 (1.6)	γ ring	422w	441.4 (1.5)	γ ring	409.3 (0.8)	β ring	430w
520.4 (5.9)	β ring	540w	523.0 (12.2)	β ring	536.5 (4.1)	β ring	540w
543.8 (14.9)	β ring + β C4═O	556m			561.5 (1.6)	γ C5−H	
559.9 (8.2)	β ring + β C2═O	576w	552.5 (14.6)	β ring	562.7 (19.6)	β ring	558m
597.8 (1.2)	γ N1−H		601.2 (12.3)	β ring	575.6 (2.4)	β ring	589w
658.1 (1.0)	γ N3−H		662.9 (1.3)	γ N3−H			
728.2 (7.0)	γ C5−H + γ C═O		720.0 (1.7)	γ C5−H	730.5 (2.2)	γ ring + γ N1−H	
743.1 (6.1)	γ C2═O + γ ring		780.0 (6.8)	γ C2═O + γ ring + γ C4═O			
774.9 (68.8)	ring breathing	786s	786.5 (21.8)	γ C4═O + γ ring + γ C2═O	763.5 (3.5)	γ C4═O + γ ring	
812.9 (9.1)	γ C4═O + γ C−H		797.3 (109.1)	ring breathing	761.8 (151.1)	ring breathing	800s
974.6 (0.8)	β ring + β N3−H				809.6 (16.8)	γ C2═O + γ N1−H	
982.3 (11.7)	γ C−H + γ ring	976w	963.6 (20.6)	β ring + β N3−H	956.8 (11.4)	β ring + β N1−H	
			989.4 (10.0)	γ C6−H + γ ring	954.8 (16.3)	γ C6−H + γ N1−H + γ ring	
990.6 (7.1)	β ring	1003w			982.6 (77.3)	β ring	990w
1091.9 (6.4)	ν ring + β N1−H + β C−H	1093w	999.5 (24.4)	β ring			1019m
1200.6 (6.6)	β C6−H + ν ring + β N−H		1096.1 (22.6)	β C−H	1100.5 (10.0)	β N1−H + β C5−H	1104m
1234.9 (29.0)	ν ring + β C−H	1234s	1150.1 (9.4)	ν ring + β C6−H	1200.9 (14.5)	β C6−H + β C5−H + β N1−H	1189s
1380.1 (28.0)	ν ring	1388s	1306.5 (18.2)	ν ring + β C−H	1288.7 (16.2)	ν ring + β C−H	
					1309.6 (92.4)	β N1−H + ν ring	1291s
1408.3 (20.4)	β N−H + ν ring	1416m	1343.7 (46.3)	β N3−H + ν ring			1367s
1420.7 (25.8)	ν ring + β N1−H + β N3−H	1444w	1386.9 (15.4)	ν ring + β N3−H + β C−H	1380.4 (16.7)	ν ring + β N1−H + β C6−H	1382m
1502.4 (27.4)	β N1−H + ν ring	1505m	1472.0 (124.4)	ν ring	1484.8 (108.6)	ν ring	1475m
			1567.2 (101.7)	ν C5═C6	1553.7 (21.0)	ν C4═O + ν C2═O + β N1−H	1560m
1667.4 (137.0)	ν C5═C6 + β N1−H	1677s	1640.8 (32.3)	ν C2═O + ν C4═O + β N3−H	1666.8 (117.1)	ν C4═O + ν ring	1640m
1733.2 (89.6)	ν C4═O + β N3−H + β C5−H	1710m	1683.4 (83.7)	ν C4═O + ν C2═O	1670.4 (113.1)	ν C4═O + ν C2═O + ν ring	
1787.8 (13.2)	ν C2═O + β N1−H + β N3−H						

[a] See Experimental Procedures for the detailed method. The vibrational mode abbreviations are as follows: ν, stretching; β, in-plane bending; γ, out-of-plane-bending. Abbreviations for observed intensities are as follows: s, strong; m, medium; w, weak.

(*5*). However, the mechanism by which UDG lowers the pK_a of uracil in the binary complex is not obvious from inspection of the 1.5 Å resolution crystal structure of uracil bound to *e*UDG at pH 8.5 (*6*). In the active site of this structure (Scheme 2), the N1 proton and O2 carbonyl groups are solvent-exposed, the uracil ring is stacked against the π-electron cloud of Phe77, and His187 is too far away to hydrogen bond with uracil O2 (4.2 Å). This arrangement would not be expected to lead to a 2.2 unit lowering of the pK_a for uracil N1, as measured in solution by NMR (*12*). A possible explanation for these differences is that the active site loop containing His187 is in dynamic equilibrium between an open state, which cannot interact with uracil O2, and a closed state that is stabilized by both uracil binding and dsAB DNA binding. From these observations, as well as the uracil-induced conformation discussed below, we infer that the enzyme is trapped in the open state in the crystal structure of the binary uracil complex. We note that the same open state is also seen in the crystal structure of the binary uracil complex of the herpes virus enzyme (*23*).

Uracil Binding Induces a Conformational Change in UDG. Most of the remaining features in the difference spectrum in Figure 7D are due to protein modes, suggesting conformational changes in UDG upon binding uracil at pH 10.2. Only some of the features can be assigned with reasonable assurance, due to overlap of certain bands, or to our rather primitive knowledge of Raman difference spectra for proteins. The sharp inflections near 1607, 1587, and 1000 cm^{-1} reflect changes in phenylalanine and/or tyrosine environments upon uracil binding, consistent with the *e*UDG−U crystal structure, which shows that uracil stacks against Phe77, with the conserved Tyr66 positioned orthogonal to the uracil plane (Scheme 2). The bands at 1557 and 881 cm^{-1} reflect tryptophan modes that gain intensity in the complex. An additional provocative result is the appearance of the sharp derivative feature at 1668/1683 cm^{-1}, which may reflect changes in the interactions of the Asn123 side chain before and after forming interactions with N3−H and O4 of uracil (Scheme 2). This assignment is suggested on the basis that there are no narrow aromatic ring modes in

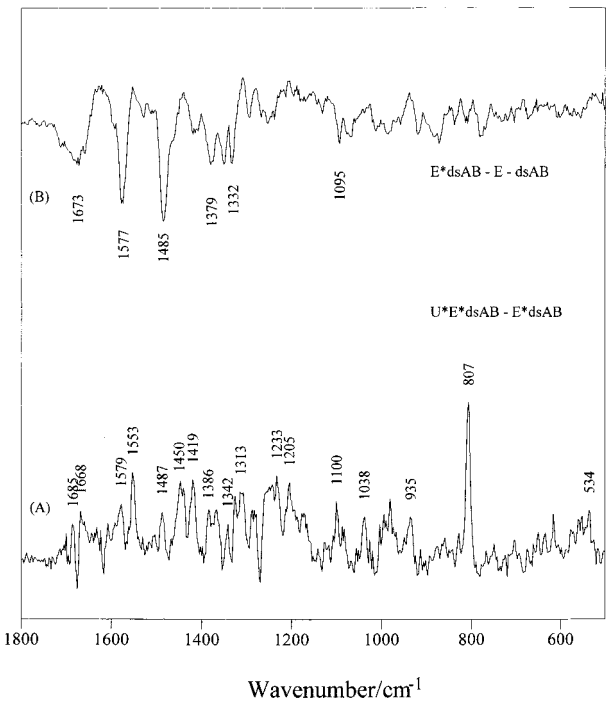

FIGURE 8: Raman difference spectrum of (A) uracil in the ternary complex with dsAB and UDG at pH 7.5 and (B) dsAB bound to UDG at pH 7.5. In spectrum A, the spectrum of the binary complex, E−dsAB, was subtracted from that of the ternary complex (E−U−dsAB). The [UDG]:[dsAB]:[uracil] ratio was 1.0:1.2:0.9, and the UDG concentration was 0.46 mM. In spectrum B, the spectra of free UDG and dsAB were subtracted from the spectrum of the binary complex E−dsAB. The [UDG]:[dsAB] ratio was 1.0:0.97, and [UDG] = 0.43 mM.

this region, and it would be unprecedented for a backbone amide band to be so narrow.

The observation of a change in secondary structure and environment for one or more Trp residues upon uracil binding is surprising, because the crystal structures of free UDG and its complex with uracil are nearly identical (*6*). However, these observations may be related to earlier solution studies where a decrease in Trp fluorescence intensity was observed upon dsU$^{\beta}$ binding (*7*). More recently, similar fluorescence changes have been measured upon uracil binding to UDG over the pH range of 6.5−10.5 (*12*). These observations indicate uracil-induced changes in the environment of one or more Trp residues, which mimic those induced by specific binding of DNA. As previously noted, Trp164 of *e*UDG is located at the end of the β3 strand, and this strand is involved in the β-zipper conformational change that occurs upon specific DNA binding (*21*). Thus, we surmise that a change in the environment of Trp164 gives rise to the changes in Raman and fluorescence signals. As noted above, these discrepancies between solution and crystallographic measurements suggest that the active site loop containing His187 of *e*UDG is in dynamic equilibrium between an open and closed state in solution, and that uracil binding shifts the equilibrium toward the closed state.

Nature of the Product Complexes with dsAB. The Raman signature of uracil in the ternary product complex with enzyme and dsAB (Figure 8A) was obtained by subtracting the Raman spectrum of the E−dsAB complex from that of the E−dsAB−U complex. This spectrum, which was obtained at pH 7.5, has many features in common with the uracil anion in the binary E−U complex at pH 10.2 (Figure 7D). The narrow nature of the uracil band at 807 cm^{-1} in Figure 8A indicates that the N1 monoanion is the dominating form of uracil in the active site of the E−dsAB−U complex, because the neutral or N3 anion species would be expected to contribute to a shoulder at 785 cm^{-1} (Table 1). The absence of an intense peak for neutral uracil at 1234 cm^{-1} strongly corroborates this point. Therefore, uracil exists as the N1 imidate form in the presence of dsAB in the UDG active site at neutral pH, confirming and extending the previous NMR observations (*5*). The upward shift of 7 cm^{-1} for the 807 cm^{-1} band, as compared with the free monoanion at pH 10.5 (Figure 7B), indicates that the active site environment promotes a modest change in the electron density distribution of the uracil ring. This change is likely due to electrostatic interactions with the active site, which may include π-stacking with Phe77, a short H bond between His187 and uracil O2 (*5*, *9*), and H bonding between the side chain of Asn123 and the N3−H and C4═O moieties of uracil (*6*).

After the release of the uracil and abasic DNA products, UDG can rebind the abasic DNA to form a stable complex with a flipped-out abasic deoxyribose ring, and this has been structurally characterized for the human enzyme (*9*). Figure 8B shows the Raman difference spectrum of the binary dsAB−UDG complex, which was obtained at pH 7.5 by subtracting the Raman spectrum of free UDG and free dsAB from that of the E−dsAB complex. This spectrum therefore reveals those features of the enzyme and dsAB that are altered upon formation of the complex. Notably, the spectrum of Figure 8B shows no evidence for changes in a Phe residue as were observed above for binding of dsU$^{\beta}$ and uracil (see Figures 4B and 7D). This provides excellent support for the previous assignment of the band at 1008 cm^{-1} in Figures 4B and 7D as arising from uracil stacking with Phe77 in the active site (Schemes 1 and 2). (We note that a negative Phe ring mode is not seen in Figure 6B due to difficulties in subtracting phosphate buffer peaks in this region.) The broad negative band near 1673 cm^{-1} in Figure 8B indicates an enzyme conformational change similar to that observed upon specific binding of dsU$^{\beta}$ in Figure 4B, but is conspicuously absent in the nonspecific complex with dsT (Figure 4A). Thus, as concluded above, an induced-fit conformational change in UDG only occurs upon formation of the specific complexes with dsU$^{\beta}$ or dsAB. With respect to conformational changes in dsAB DNA upon binding UDG, the same overall increase in the level of base stacking is observed that was seen with dsT and dsU$^{\beta}$. This conclusion is in agreement with previous assessments of dsAB binding to UDG, in which fluorescence quenching was observed for the adenine analogue 2-aminopurine placed across from the abasic site in duplex DNA (*24*).

CONCLUSIONS

The Raman results present the following picture of the events during catalytic turnover of UDG. (1) In the earliest event in damage site recognition, UDG binds nonspecifically to DNA (Figure 3A,B). This interaction is characterized by an overall increase in the level of base stacking of the DNA, as indicated by Raman hypochromism (Figure 4A). The increased level of stacking could represent enzyme-induced strain in the duplex, possibly caused by a small amount of

DNA bending. Such nonspecific binding may play a role in facilitating the subsequent uracil flipping step. (2) Upon location of the damaged site, the uracil is extruded from the double helix into the active site of UDG. Although the damage specific complex with the extrahelical uracil shares the same increased base stacking signature as observed for the nonspecific complex, additional Raman features appear which indicate a conformational change in the enzyme, and intimate uracil stacking with Phe77 (Figures 3C, 3D, 4B, and 8A). (3) The uracil ring in the substrate oligonucleotides retains its quasi-aromatic electronic structure, with only a small electron reorganization in the ground state complexes. In contrast, large changes in H bonding of the uracil C═O groups are observed, which likely weakens the *N*-glycosidic bond in the ground state (Figures 5 and 6). (4) Upon cleavage of the glycosidic bond, the uracil product is bound only in the N1 monoanion form at pH 7.5 ($pK_a^{N1} = 6.4$, which is 3.4 units lower than in solution). (5) Upon ordered release of the abasic DNA product, the uracil N1 pK_a is raised by 1.2 units ($pK_a^{N1} = 7.6$) (*12*), and the product is therefore bound as a mixture of the monoanion and neutral species, which weakens its interaction with the enzyme, facilitating uracil release (*12*). (6) Upon release of uracil, the abasic DNA product may rebind to the enzyme in a competitive manner with substrate, which results in the same increased level of DNA base stacking as observed for the nonspecific and dsU^{β} complexes (Figure 8B). Whether this dsAB−UDG product complex has a sufficiently significant lifetime that could lead to ordered passage of the abasic site to the next enzyme in the base excision repair pathway is currently being investigated by kinetic approaches.

ACKNOWLEDGMENT

We thank the Ohio Supercomputer Center (Project PDS0183) for part of the calculation work carried out on T90 vector processor.

SUPPORTING INFORMATION AVAILABLE

Tables 1 and 2 providing assignments of UDG and the double-stranded DNA 11mer Raman spectra, respectively. This material is available free of charge via the Internet at http://pubs.acs.org.

REFERENCES

1. Parikh, S. S., Mol, C. D., Hosfield, D. J., and Tainer, J. A. (1999) *Curr. Opin. Struct. Biol. 9*, 37−47.
2. Mosbaugh, D. W., and Bennett, S. E. (1994) *Prog. Nucleic Acid Res. Mol. Biol. 48*, 315−370.
3. Drohat, A. C., Jagadeesh, J., Ferguson, E., and Stivers, J. T. (1999) *Biochemistry 38*, 11866−11875.
4. Drohat, A. C., Xiao, G., Tordova, M., Jagadeesh, J., Pankiewicz, K. W., Watanabe, K. A., Gilliland, G. L., and Stivers, J. T. (1999) *Biochemistry 38*, 11876−11886.
5. Drohat, A. C., and Stivers, J. T. (2000) *J. Am. Chem. Soc. 122*, 1840−1841.
6. Xiao, G., Tordova, M., Jagadeesh, J., Drohat, A. C., Stivers, J. T., and Gilliland, G. L. (1999) *Proteins 35*, 13−24.
7. Stivers, J. T., Pankiewicz, K. W., and Watanabe, K. A. (1999) *Biochemistry 38*, 952−963.
8. Parikh, S. S., Walcher, G., Jones, J. D., Slupphaug, G., Krokan, H. E., Blackburn, G. M., and Tainer, J. A. (2000) *Proc. Natl. Acad. Sci. U.S.A. 97*, 5083−5088.
9. Parikh, S. S., Mol, C. D., Slupphaug, G., Bharati, S., Krokan, H. E., and Tainer, J. A. (1998) *EMBO. J. 17*, 5214−5226.
10. Lindahl, T., Ljungquist, S., Siegert, W., Nyberg, B., and Sperens, B. (1977) *J. Biol. Chem. 252*, 3286−3294.
11. Fasman, G. D. (1975) *Handbook of Biochemistry and Molecular Biology: Nucleic Acids*, 3rd ed., Vol. 1, CRC Press, Boca Raton, FL.
12. Drohat, A. C., and Stivers, J. T. (2000) *Biochemistry 39*, 11865−11875.
13. Dong, J., Dinakarpandian, D., and Carey, P. R. (1998) *Appl. Spectrosc. 52*, 1117−1122.
14. Kim, M., Owen, H., and Carey, P. R. (1993) *Appl. Spectrosc. 47*, 1780−1783.
15. Frisch, M. J., et al. (1998) *Gaussian 98*, Gaussian, Pittsburgh, PA.
16. Harada, I., and Takeuchi, H. (1986) in *Advances in Spectroscopy* (Clark, R. J. H., and Hester, R. E., Eds.) pp 113−175, Wiley, New York.
17. Overman, S. A., and Thomas, G. J. J. (1998) *Biochemistry 37*, 5654−5665.
18. Peticolas, W. L., Kubasek, W. L., Thomas, G. A., and Tsuboi, M. (1987) *Biological Applications of Raman Spectroscopy* (Spiro, T. J., Ed.) pp 81−134, Wiley, New York.
19. Thomas, G. J., Jr., and Wang, A. H.-J. (1988) *Nucleic Acids Mol. Biol. 2*, 1−30.
20. Benevides, J. M., Chan, G., Lu, X.-J., Olson, W. K., Weiss, M. A., and Thomas, G. J., Jr. (2000) *Biochemistry 39*, 537−547.
21. Putnam, C. D., Shroyer, M. J. N., Lundquist, A. J., Mol, C. D., Arvai, A. S., Mosbaugh, D. W., and Tainer, J. A. (1999) *J. Mol. Biol. 287*, 331−346.
22. Thomas, G. J., Jr., and Tsuboi, M. (1993) *Adv. Biophys. Chem. 3*, 1−70.
23. Savva, R., McAuley-Hecht, K., Brown, T., and Pearl, L. (1995) *Nature 373*, 487−493.
24. Stivers, J. T. (1998) *Nucleic Acids Res. 26*, 3837−3844.

BI001437M